Electronic Supplementary Material (ESI) for RSC Advances.
This journal is © The Royal Society of Chemistry 2021

Supplementary Information for

Sub-nanograins metal based high efficiency multilayer reflective optics for high energies

Arindam Majhi[1,2], Maheswar Nayak[1,2*], Paresh Chandra Pradhan[3], Suvendu Jena[4], Anil Gome[5], Manvendra Narayan Singh[1], Himanshu Srivastava[1], Varimalla Raghvendra Reddy[5], Arvind Kumar Srivastava[1,2], Anil Kumar Sinha[1,2], Dinesh Venkatesh Udupa[2,4] and Ullrich Pietsch[6]

[1]Synchrotrons Utilization Section, Raja Ramanna Centre for Advanced Technology, Indore 452013, India

[2]Homi Bhabha National Institute, Anushakti Nagar, Mumbai 400094, India

[3] Advanced Photon Source, Argonne National Laboratory, Argonne, IL 60439, USA

[4]Atomic and Molecular Physics Division, Bhabha Atomic Research Centre, Mumbai 400085, India

[5]UGC-DAE Consortium for Scientific Research, University Campus, Khandwa Road, Indore 452001, India

[6]Universität Siegen, Walter-Flex-Strasse 3, Siegen, 57072, Germany

*Corresponding author: mnayak@rrcat.gov.in

SI1: Theoretical calculations to understand material systems for soft gamma-ray ML reflective optics

In the soft gamma-ray spectrometer, the main challenge is requirement for efficient optics to deliver sufficient amount of photon flux to improve signal-to-noise ratio. This is because of the weak signal strength of emitted gamma-rays from distance stellar objects as well as remnant radioactive isotopes in nuclear spent-fuel. This stipulates the need for a better material system for ML mirror that can provide both high peak reflectance as well as high integrated reflectance (area under the Bragg peak). For optical consideration, only four selected material systems are chosen for optical consideration (Fig. S1), owing to their ability to form a low interfacial imperfection at ultra-short period, which is required for such a high energy application. According to classical wave physics, incoherent scattering in the soft gamma-ray region does not affect the intensities of ML optics at Bragg angle[1], so the amplitude of the Bragg peak can be calculated theoretically using the wave model[2]. Fig. S1 (a) demonstrates the tolerable range of interface width (σ) in different MLs with period d = 1.86 nm calculated at 300 keV. The achievable σ reported earlier on WC/SiC ML optics[1] is 0.275 nm (vertical dotted line), whereas that in the present study on W/B_4C ML system is 0.27 nm (vertical dashed line). At the marked values of σ, the calculated reflectivities of WC/SiC, WC/B_4C, W/B_4C and W/Si MLs are nearly the same within 1%. However, in order to understand the role of optical contrast on photon flux, Fig. S1 (b) shows that the onset of saturated peak reflectivity (marked by arrows) is material dependent. For a better understanding of Fig. S1 (b), it is noted that the ideal density contrast of WC/SiC, WC/B_4C, W/B_4C and W/Si has to be 12.42 g cm^{-3}, 13.11 g cm^{-3}, 16.78 g cm^{-3} and 16.97 g cm^{-3}, respectively[3]. Thus, ideal density contrast in W/B_4C is ~35 % higher compared to WC/SiC system. It is inferred from Fig. S1 (b) that the higher the density contrast, the lower is the number of layer pairs, N, reaching the onset of saturated reflectivity. The latter occurs at N ~190 and ~250 for W/B_4C and WC/SiC, respectively. Thus, W/B_4C has higher integrated reflectance and provides a higher photon flux compared to both WC/SiC and WC/B_4C. Further, comparing W/B_4C with W/Si, the achievable interfacial perfection in W/B_4C is anticipated better because of interfacial diffusion and/or reactivity of Si with metal[4-6]. Also, the integrated 1st Bragg peak intensities (FWHM × peak reflectivity) is calculated with two ML systems (WC/SiC and W/B_4C) calculated by considering the periodicity 1.86 nm, N=400, ideal mass densities and zero roughnesses of materials at a photon energy of 378 keV. Calculations are done by considering the step size of 0.0001°. The calculated integrated 1st Bragg peak intensity of W/B_4C ML is ~ 40% greater compared to the WC/SiC ML.

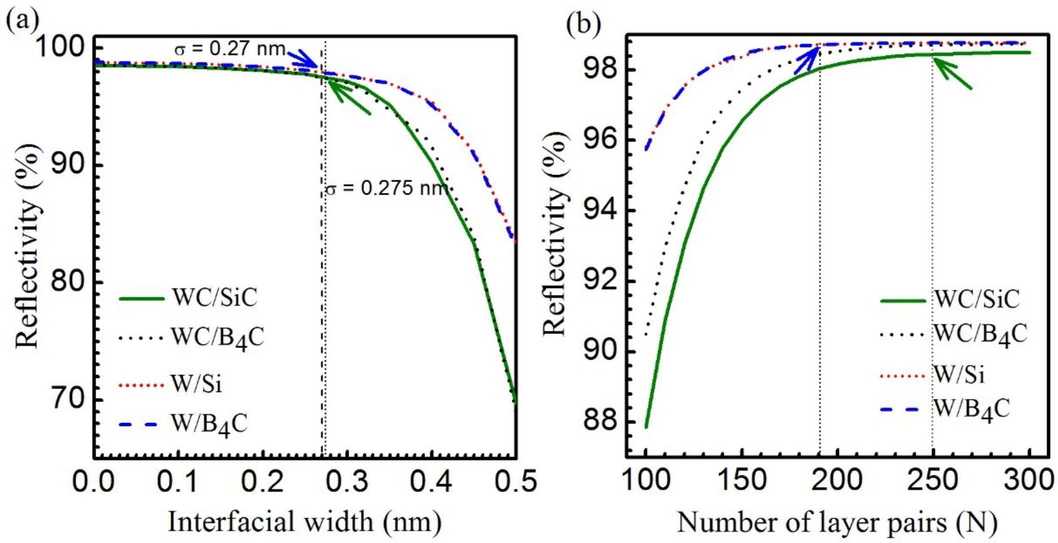

Fig. S1 Optical performance of MLs with four different material systems (WC/SiC, WC/B_4C, W/Si and W/B_4C) calculated by considering ideal mass densities of materials at a photon energy of 300 keV. Calculations are done by considering the step size of 0.0001° and instrumental angular resolution (Δθ) of 0.0001°. (a) Peak reflectivity of the first order Bragg peak as a function of σ. The calculations are performed for MLs with N = 400, d = 1.86 nm and the thickness ratio, Γ = 0.505. The vertical dotted line indicates the value of σ = 0.275 nm of previously reported WC/SiC ML optics[1] and the vertical dashed line represents the interfacial width 0.27 nm of W/B_4C ML in the present study. The positions of the olive and blue colored arrows indicate the corresponding calculated reflectivities at the marked value of σ. (b) Peak reflectivity of the first order Bragg peak as a function of N indicating material dependence of onset of saturated peak reflectivity (marked by arrows).

SI2: Crystallite size considering W (211) orientation

Figure S2 shows the measured GIXRD spectra considering W (211) orientation as well as W (220) orientation for ML-2 at 15.6 keV with incident angle at 4.5°. Since, the intensities are smaller, so we measured only in out-of-plane direction. Since, the intensities of W (220) is very weak, so it is difficult to extract the crystalline size accurately using W (220). Hence, here we call very weak W

(220) along with other possible peaks, which we unable to measure due to low intensities as random orientation in the schematic (Figure 4 in the manuscript).

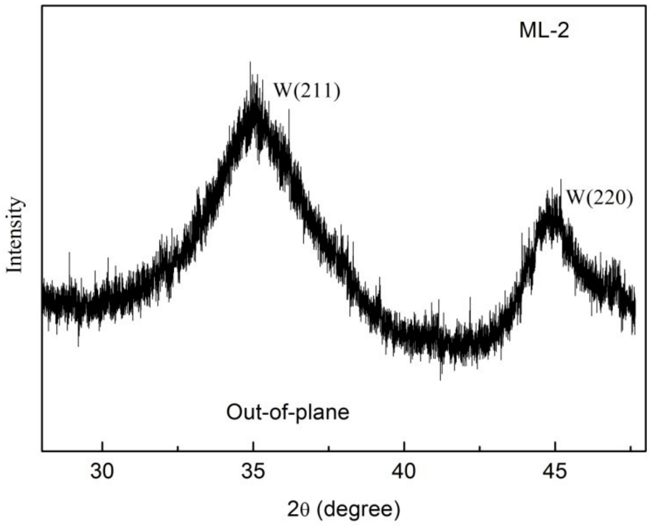

Fig. S2: GIXRD spectra for ML-2 at 15.6 keV with incident angle at 4.5°. It shows that the W (211) orientation as well as W (220) orientation.

The measured data of W (211) having weak intensities for all three samples (ML-1, ML-2 and ML-3) in the out-of-plane direction along with the fitted curves are as shown in figure below. The approximate average crystallite sizes in out-of-plane direction obtained for W (211) is given in Table, which is ~1 nm range.

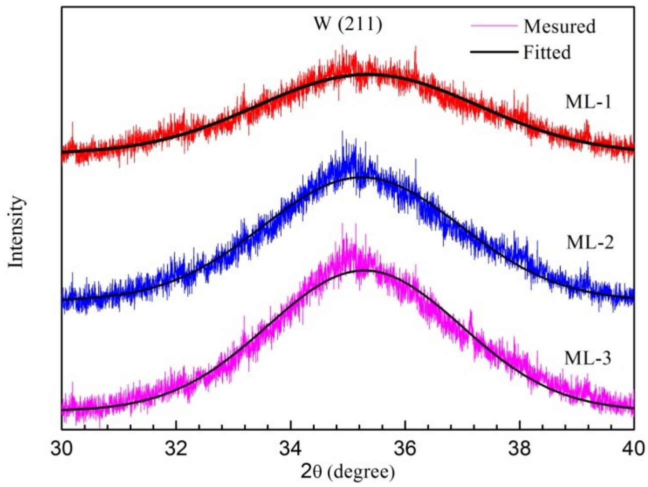

Fig. S3: Measured and fitted GIXRD profiles of W (211) diffraction of three MLs at energy 15.6 keV in out-of-plane direction.

Table: Out-of-plane crystallite size considering W (211)

Sample Number	Peak position (2θ) of W	Crystallite size

	(211) (degree)	
ML-1	35.34	0.94 nm
ML-2	35.24	1.05 nm
ML-3	35.28	1.07 nm

SI3: Analysis of Residual stress in ML stack

The residual stress is another important factor that needs to be characterized in such ML mirrors having large values of N for long term stability.

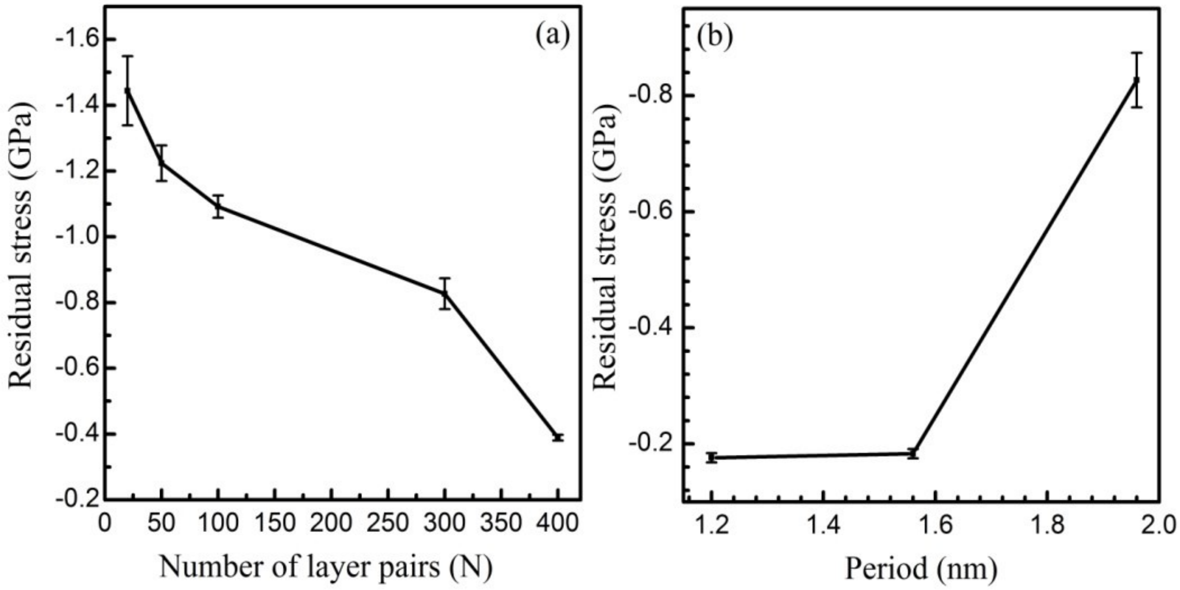

Fig. S4 The measured total residual stress in W/B_4C ML films as a function of N from 20 to 400 at a fixed period d ≈ 1.9 nm is shown in the figure (a). The details analysis of residual stress as function of number of layer pairs are reported elsewhere[7]. Fig. S4 (a) is reproduced from A. Majhi et al., J. Applied Physics, 2018, 124, 115306, with the permission of AIP Publishing as the reference of our earlier work on total residual stress in ML optics. The total residual stress is compressive in nature. Total residual stress decreases with increasing N. For N = 400, total residual stress of ML film is -0.389 GPa. It is also observed that at a fixed number of layer pairs N=300, as the periodicity decreases, the residual stress decreases as shown in figure (b). Previously Fernandez Perea et al.[8] measured the total residual stress WC/SiC ML with varying periodicity, number of layer pairs and different Γ ratio. They measured the total residual stress is compressive. The total compressive residual stress is ~0.55 GPa for ML with N= 300 (d = 1 nm and Γ=0.4) and the total compressive residual stress is ~0.2 GPa for N= 500 (d = 1.5 nm and Γ=0.4). In the present study, for W/B_4C ML the total residual stress is -0.827± 0.047 GPa for N = 300 and -0.389 ± 0.009 GPa for N = 400. The measured stress in W/B_4C ML with N = 400 is in the tolerable range for soft gamma ray multilayer optics.

SI4: Study of Period Uniformity

In the soft gamma-ray region, ML mirrors to be operated at extremely small glancing incidence angles of a few to several milli-radians, so it is important to characterize the lateral uniformity of d of the ML mirrors.

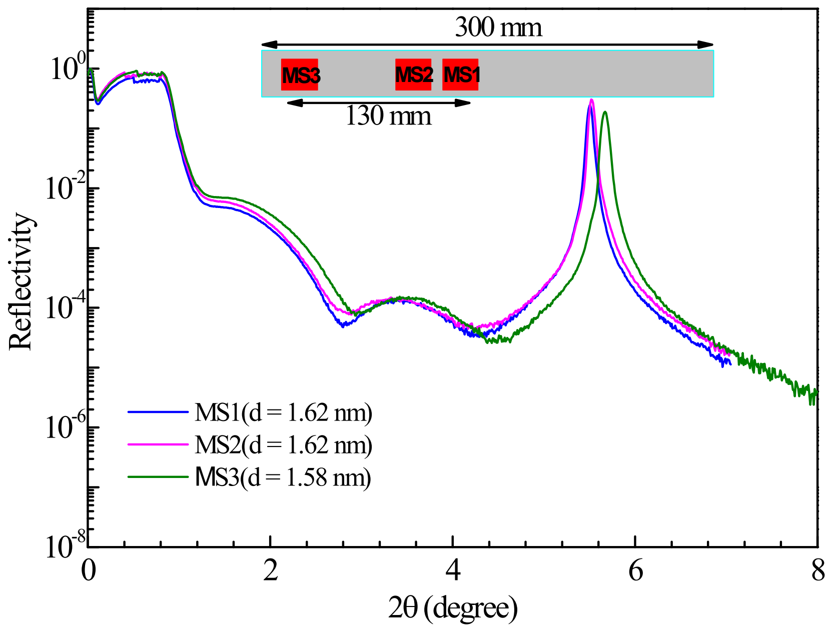

Fig. S5 Measured XRR data (at Cu K_α energy)of three W/B_4C ML samples (MS1, MS2, MS3) with a fixed N= 300 fabricated in one run deposition. The three samples are mounted at three different distances starting from middle position towards one end within 130 mm length scale in a 300 mm Substrate holder as shown in inset of the figure. The periodicity decreases slightly from centre of the substrate holder to the end of the one side in a regular manner with respect to the distance from the centre of the substrate holder. This is due to the spatial variations of deposition rate across the cathode (500 mm length) material. It is anticipated that density of plasma is more at the centre of the cathode, and decreases towards the ends of the cathode in a magnetron sputtering. The XRR data shows that the period non-uniformity over 130 mm length (from centre to one end of substrate holder) is ~ 2.5 %. It is anticipated that the spatial variation of the sputtered atoms is nearly symmetrical from centre towards both ends of cathode. So, by properly arranging a masking arrangement in front of cathode with slightly symmetrically tapering of mask towards centre would neutralize the difference of spatial distribution of sputtered atoms coming from the centre and from the both ends of cathode through the tapered mask. This will certainly significantly further improve lateral uniformity of period without altering the quality of ML optics in terms of layer structure, interface width and residual stress in the ML stack.

SI5: Measured Optical performances and analysis

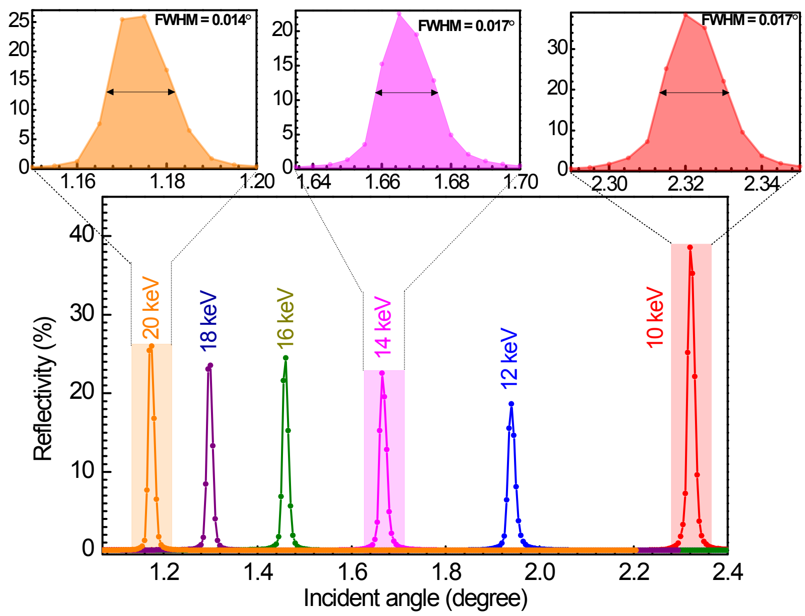

Fig. S6 Measured optical performances of W/B_4C ML (ML-2) with d = 1.55 nm and N = 400 in the energy range 10-20 keV. The percent of reflectivities (in linear scale) at first Bragg peak as a function of the incident angle at different selected energies are shown in lower part of the figure. At energy 10 keV the measured 1st Bragg peak reflectivity is ~ 39 %. At 10 keV, by comparing with ML with d=1.86 nm having reflectivity ~64 % (ML-1, discussed in manuscript), the decrease of reflectivity is due to q-dependency of reflectivity along with the decrease of density contrast (13. 1 g/cc) as well as slightly increase of interface width (~ 0.285 nm). The variations of measured reflectivity with the energies follows nearly a similar trend for ML-1, ML-2 and ML-3 (d=1.23 nm). When the energy increases to 12 keV reflectivity decreases to ~ 18 % which is due to the presence of W L_{II}-edge at 11.544 keV. After that the reflectivity again increases with increasing the incident photon energy away from the W L_{II}-edge at 11.544 keV. The top s shows the enlarge version of measured 1st order Bragg peak indicating more clarity about FWHM at three different energies as 10 keV, 14 keV and 20 keV respectively. E/ΔE is calculated using $E/\Delta E = \tan(\theta_{Bragg}) \times (1/$ FWHM of the

Bragg peak). The measured energy resolutions (ΔE) of Bragg are 75 eV, 143 eV and 243 eV corresponding to the energies at 10 keV, 14 keV and 20 keV respectively. The variations of the measured optical properties (first order reflectivity and resolution) agree well with the theoretical values considering the respective derived model.

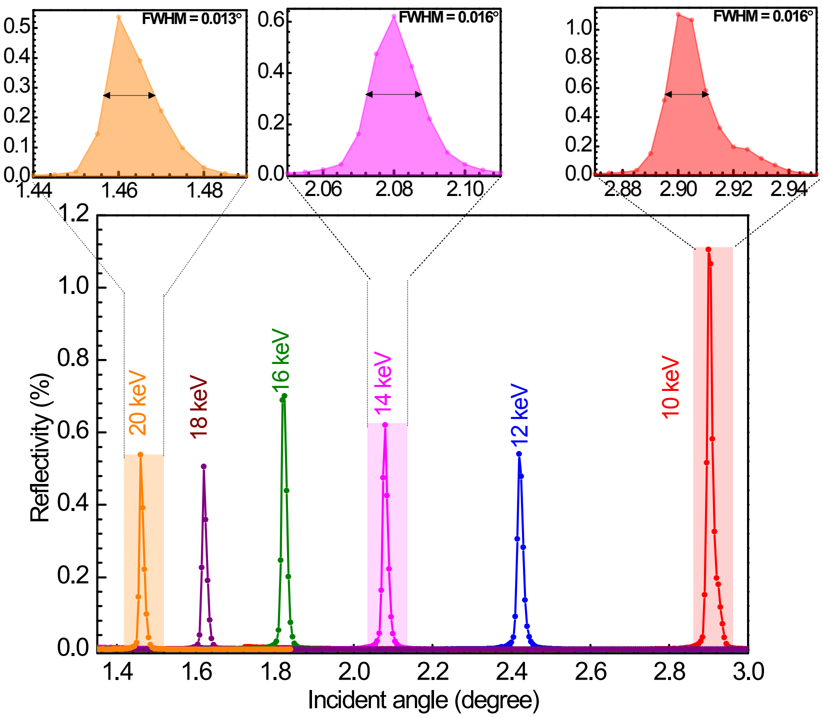

Fig. S7 Measured optical performances of W/B_4C ML (ML-3) with d = 1.23 nm and N = 400 in the energy range 10-20 keV. The percent of reflectivities (in linear scale) at first Bragg peak as a function of the incident angle for selected energies are shown in lower part of the figure. At energy 10 keV the measured 1st Bragg peak reflectivity is only ~ 1.1 %. For comparison with ML-1 and ML-2, the measured reflectivity drastically drops for ML-3 due to q-dependency of reflectivity along with significantly decreases of density contrast (6.5 g/cc) at the interface along with increase of interfacial width (0.325 nm). The significantly decrease of density contrast along with increase of interfacial width are due to formation of quasi-continuous layer of B_4C because of its low thickness (0.33 nm). When the energy increases away from 10 keV the optical performance follow the same trend as other two ML mirrors. The top figures show enlarge 1st order Bragg peak indicating more clarity about the measured angular resolution of Bragg peaks at three selected energies. The variations of the measured optical properties (reflectivity and resolution) agree well with the theoretical values considering the respective derived model.

SI6: Details of calculation of soft gamma-ray optical performance

The predicted soft gamma-ray optical performances (1st order Bragg peak reflectivity) of three ML mirrors (ML-1, ML-2 and ML-3) with varying instrumental angular resolution (Δθ) are calculated at photon energies of 384 keV (ΔE = 3 keV) and 378 keV (ΔE = 9.8 keV) using 'IMD' code under 'XOP' software package[2]. The calculation is done with an angular step size 0.1 mdeg using measured structural parameters of MLs derived from hard x-ray data and by extrapolation of known optical properties of materials. The calculations of the reflected intensities at the multiple discrete energies in the bandwidth interval with energy step of 0.3 keV (0.5 keV) for ΔE = 3 keV (9.8 keV) are averaged to account the respective resolution of incident photon energy. It is noted that Bragg reflection of such high energy peak from ML mirror appears at very low Bragg angles. For example, a typical reflectance band pass (FWHM) of the first order Bragg peak (position at~50.4 mdeg) from ML with d =1.86 nm and having Δθ =0.024 mdeg is of the order of ~0.5 mdeg at energy 384 keV. So, the Δθ needs to be much lower than FWHM of the Bragg peak.

References:

1 M. Fernandez-Perea, M. A. Descalle, R. Soufli, K. P. Ziock, J. Alameda, S. L. Baker, T. J. McCaville, V. Honkimaki, E. Ziegler, A. C. Jakobsen, F. E. Christensen, and M. J. Pivovaroff, *Phys. Rev. Lett*. 2013, **111**, 027404.

2 D. L. Windt, IMD version 5.0, 2013, See http://www.rxollc.com/idl/index.html.

3 B. L. Henke, E, M. Gullikson, J. C. Davis, *At. Data and Nucl. Data Tables* 1993**, 54**, 181-342, See http://henke.lbl.gov/optical_constants/.

4 C. Eberl, T. Liese, F. Schlenkrich, F Doring, H. Hofsass, H.-U. Krebs, *Appl. Phys. A*, 2013, **111**, 431-437.

5 Zhang Jin-Shuai; Huang Qiu-Shi; Jiang Li; Qi Run-Ze; Yang Yang; Wang Feng-Li; Zhang Zhong; Wang Zhan-Shan. *Acta Physics Sinica*, 2016, **65**, 086101.

6 M. Jergel, E. Majkova, V. Holy, S. Luby, R. Senderak, *Il Nuovo Cimento*, 1997, **19**, 439-445.

7 A. Majhi, M. Dilliwar, P. C. Pradhan, S. Jena, M. Nayak, M. N. Singh, D. V. Udupa, N. K. Sahoo. *J. Appl. Phys*., 2018, **124**, 115306.

8 M. Fernandez-Perea, M. J. Pivovaroff, R. Soufli, J. Alameda, P. Mirkarimi, M. A. Descalle, S. L. Baker, T. McCarville, K. Ziock, D. Hornback, S. Romaine, R. Bruni, Z. Zhong, V.

Honkimaki, E. Ziegler, F. E. Christensen, and A. C. Jakobsen, *Nucl. Instr. Meth. Phys. Res. A* 2013, **710**, 114-119.